Blazar Microvariations

Cameron Pittman

Senior Honors Thesis

Advisor: Dr. Robert Knop
Vanderbilt University
Department of Physics and Astronomy

Spring 2009

Abstract

In November 2006, the authors collected data on blazars PKS 0537-441, PKS 0447-439, and PKS 0208-5121 from the Cerra Tololo Inter-American Observatory in Chile. All three blazars are tested for microvariability, first by comparing relative magnitudes against unvarying stars, then through power spectrum analysis. The authors used GNU Scientific Library tools for the Fourier transforms needed for power spectrum analysis.

Fourier transforms break down data into series of periodic functions. Running power spectra quantitatively illuminate periodicity and variability in data. The authors tested power spectra by using well-defined functions to better understand power spectra analysis. Through light curve analysis and power spectra analysis, the authors found PKS 0537-441 showed microvariability, PKS 0208-512 most likely did not show microvariability, and PKS 0447-439 did not show microvariability.

Table of Contents

Physical Properties and Previous Models

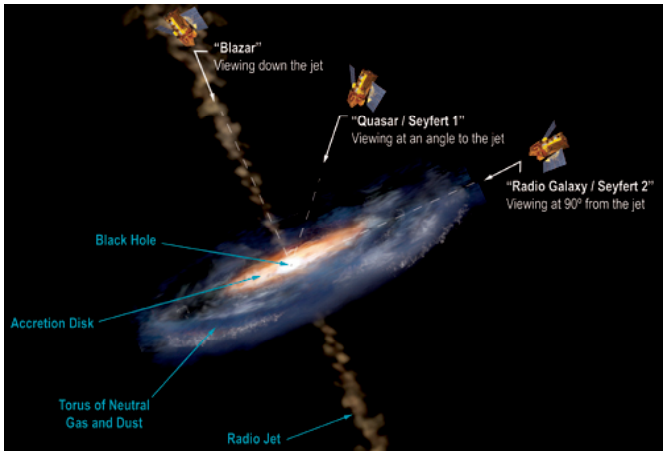

Figure 1 – An illustration of an AGN (Simonnet). Note that to be a blazar, an AGN's relativistic jet must be aimed directly at the observer. Different categories of AGNs are suspected of being the same intrinsic object viewed at different angles.

Blazars are a class of Active Galactic Nuclei (AGN), which combine BL Lacertae and Optically Violently Variable (OVV) objects. AGNs are currently modeled as active supermassive black holes in a galaxy's core. Energy from infalling gas and dust generate an accretion disk, which generates an AGN's massive luminosity. Some AGNs also produce high-energy relativistic jets. Blazars are unique in that their jets point at Earth (Krolik, 1999).

Interestingly, we see a sharp rise in AGN luminosity near z = 2.5 indicating AGNs were more active in the young universe (Krolik, 1999). As such, we believe AGNs actively shape galaxy formation, though the exact mechanism is unknown. We do know, however, that a large percentage of modern galaxies contain supermassive black holes in their cores. It is not unreasonable to believe some of these modern galactic cores were at one point active.

AGNs are some of the most luminous objects in the observable universe. Often, radiation from the AGN outshines the rest of the galaxy. While most extended galaxies have a luminosity density of something like 10^{44} erg s^{-1} pc^{-3}, AGNs may reach luminosity densities of up to 10^{48} erg s^{-1} pc^{-3} (Krolik, 1999).

Relativistic jets are volatile and show variability in the span of a few minutes, hours, or days, which we call microvariability (Ghosh, 2000). Some blazars show changes over longer timescales, such as weeks or years (Kraus, 1999). Microvariations may be caused by either intrinsic or extrinsic mechanisms. Extrinsic mechanisms mainly include scintillations in the interstellar medium (ISM), which cause diffraction and refraction effects leading to microvariability (Wagner & Witzel, 1995). However, optical wavelengths (such as the R-band used in this study) are not heavily subjected to ISM scintillation. We would also expect that if ISM scintillations cause microvariability, any variability we see would be heavily wavelength dependent, which studies have found (Meier et al, 2001). It has also been proposed that instabilities in the accretion disk lead to extrinsic variations (Wiita, 1996).

The most plausible proposed mechanism for intrinsic variation is shocks in an AGN's relativistic jets. Relativistic jets radiate through synchrotron radiation, which occurs when charged particles are caught and accelerated in magnetic field lines. Relativistic jets also contain blobs of high-energy plasmas. When two such blobs collide, a shock occurs, which could be the source for intrinsic variability (Meier et al, 2001).

Any intrinsic variability we find gives us direct information about the emission source. No intrinsic effect can coordinate faster than the object's size divided by the speed of light, which is the time needed to send a signal from one side of the object to the other. Therefore if a large light source (like an AGN) varies in brightness because of some intrinsic mechanism, it takes some time, Δt, to observe an entire variation. By comparing the speed of light and the time required for an observer to see a full intrinsic variation, we can get an upper limit for the size of the object with the relation,

$$R_{AGN} \leq c \cdot \Delta t \,. \qquad (1)$$

Data Collection

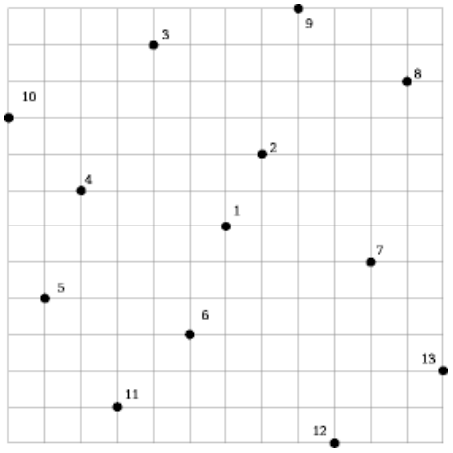

Figure 2 - Dither Pattern - The numbers represent a sequential change in position from one exposure to the next. Horizontal grid marks correspond to 0.5s RA, while vertical grid marks correspond to 5" DEC. For example, a movement from position 1 to 2 is (+0.5s, +10").

Object	Night	Exposure Time / Image (s)	Exposures / Dither	Total Images
PKS 0537-441	2006-11-23	30	20	374
PKS 0447-439	2006-11-24	30	20	540
PKS 0208-512	2006-11-25	120	5	162
UGC 0842	2006-11-26	30	20	329

Table 1 – Objects, images, and exposures

Object	Redshift (z)	RA	DEC	"Typical" Magnitude
PKS 0537-441	0.090	05h 38m 50.36s	-44d 05m 08.93s	15.96 (B)
PKS 0447-439	0.107	04h 49m 24.7s	-43d 50m 09s	16.0 (V)
PKS 0208-512	1.003	02h 10m 46.20s	-51d 01m 01.89s	16.93 (V)
UGC 0842	0.045	01h 18m 53.64s	-01d 00m 06.6s	15.0 (B)

Table 2 – Object Information. From Set of Identifications, Measurements, and Bibliography for Astronomical Data (SIMBAD) (http://simbad.u-strasbg.fr/simbad/)

Dr. Robert Knop and I traveled to the Cerra Tololo Inter-American Observatory in Chile where we collected data over the course of four nights from 23 to 26 November 2006. We used the 1.0m reflecting telescope to track four objects over the course of the four nights; we tracked a single object each night. As we were tracking quick changes in each object, we used only the R-band filter in order to minimize the time between exposures.

We picked target objects that were microvariability candidates. Previous observations of PKS 0208-512 showed microvariability (Romero et al, 2002). PKS 0537-441 also might have shown previous microvariability (Romero et al, 2000) (Dolcini et al, 2005). PKS 0447-439 and UGC 0842 were chosen as likely microvariability candidates.

In order to compensate for pixel bias, where pixels show different inherent properties, we engaged a dither pattern to guarantee that objects moved across the frame.

We systematically slightly changed the field of view over the night so that no object stayed centered on the same pixel for all images. We collected between five and twenty images at each dither position before changing to a new one. We cycled through the dither pattern about twice each night. Figure 2 shows the dither pattern we used.

We primarily focused on relative changes in each object and did not compare objects between nights. Thus, we shaped exposure time on each object to make data analysis easier. Table 1 gives a lists dates, objects, exposure times, and exposures per dither.

Please note that while we observed four different objects, this paper will only focus on three, PKS 0537-441, PKS 0447-439, and PKS 0208-512. Computer malfunctions prevented us from including the analysis of UGC 0842 in this paper.

The CTIO 1.0m telescope uses the Y4KCam, which provides a resolution of 4064 by 4064 pixels and a 20 by 20 square arcminute field of view. It reads out data to four quadrants on a CCD chip (Pogge, 2007).

CCD chips collect data by turning photon hits into digital pixel values. CCD chips have a large matrix, or array, of pixels. As photons hit each pixel, each pixel registers the hit by increasing its charge with a photoelectron. In reading out data from the chip to the computer, charge is moved from each pixel across the chip to a readout column, and then through an amplifier into the computer, which registers the charge as counts. Pixels with higher counts appear whiter than pixels with lower counts.

Data Reduction

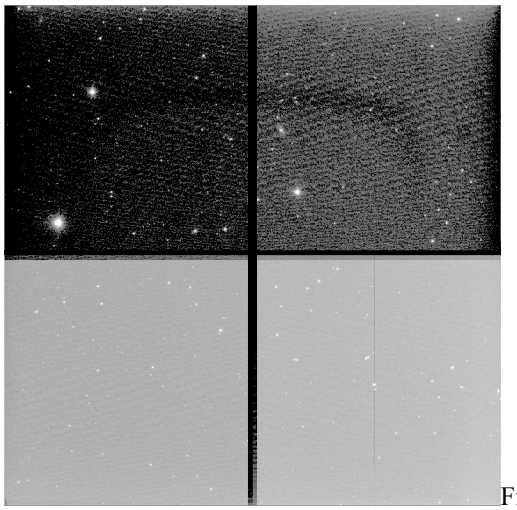
Figure 3 – Raw Image. Note the black overscan regions.

Overscan, Trim, and Knit

The Y4KCam records data in four quadrants, each of which has its own amplifier and overscan regions. Each amplifier reads out data from pixels after all data have been collected, creating overscan regions. Overscan regions contain fake data. No photons strike these regions, and thus any charge the amplifier reads is only its inherent bias. We read the overscan regions and subtract the inherent bias we find from the actual data. Our chip used four amplifiers, which become apparent in the raw image in figure 3.

The horizontal and vertical black bars are the overscan regions. Close inspection of the overscan regions show they are split in half, with each half corresponding to a different quadrant's amplification bias.

Using Dr. Knop's overscan correction program, we were able to subtract the amplifier bias as measured from the overscan region. Once corrected for, the overscan region has no purpose. Thus, following overscan correction, each image was carefully trimmed into the four quadrants containing data, then knitted back together without overscan regions.

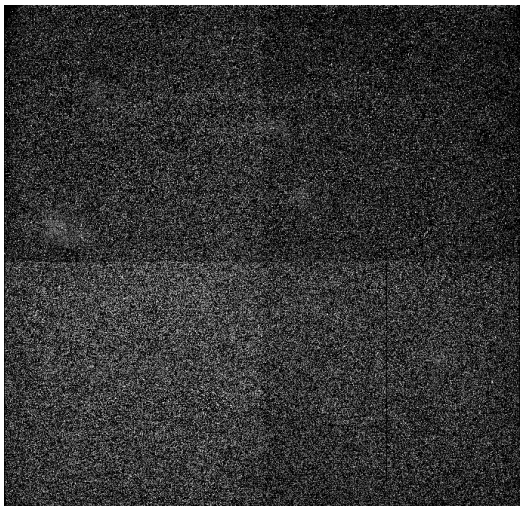
Figure 4 – Super flat. Notice that individual objects are not resolved.

Zero

After the overscan correction, there may still be residual pixel-to-pixel zero offset bias variations. To correct for the zero offset bias, we took zero second exposure images. By taking a few of these images and averaging them together, we were able to find an adequate zero value for each pixel. We zero corrected our data by subtracting the zero image from each image.

Constant Multiplication

We multiplied each quadrant by a different reference constant to equalize their units. Different amplifiers react to photoelectrons differently, generating a gain. We measure the gain in electrons per count. We determined the relative gain for each quadrant by computing the average number of counts in a dark area of the sky. By comparing these constants, we were able to determine each amplifier's gain. We then accounted for each quadrant's relative gain through constant multiplication to bring each sky background to the same level. It is important to note that the gain differences were very small and under five percent different between quadrants.

Flatfield

Flatfields are exposures of unfocused, or flat, sources, with the idea being that each pixel receives the same number of photons. Taking exposures of flat fields of view reveal intrinsic efficiencies of each pixel when exposed to light. If every pixel reacted to light in the same manner, a flatfield image would show every pixel at the same value, which unfortunately does not happen.

There are various types of flats. The ones we used include dome, twilight, and super flats. Dome flats use an illuminated white screen in the telescope's dome. Twilight flats use the flat sky at twilight. Super flats median many images together, some with stars, to produce a flatfield. In creating out super flat, we used one image from each dither from each night to create a large spread of objects. Doing a median with many

objects spread over the entire image nulls individual objects and creates a smooth image. This may be done in lieu of using twilight or dome flats.

We neglected dome flats in lieu of using twilight or super flats for empirical reasons. Pixels may have varying efficiencies as a function of wavelength. Twilight or dome flats may be colored differently than the night sky. As such, we get smoother images by using a flatfield with the same color as the sky. Figure 4 gives an example of a super flat. Therefore, we used twilight and super flats rather than dome flats.

By dividing the data by a flatfield, we correct for the intrinsic efficiency of each pixel when exposed to light.

Reduced Image Examples

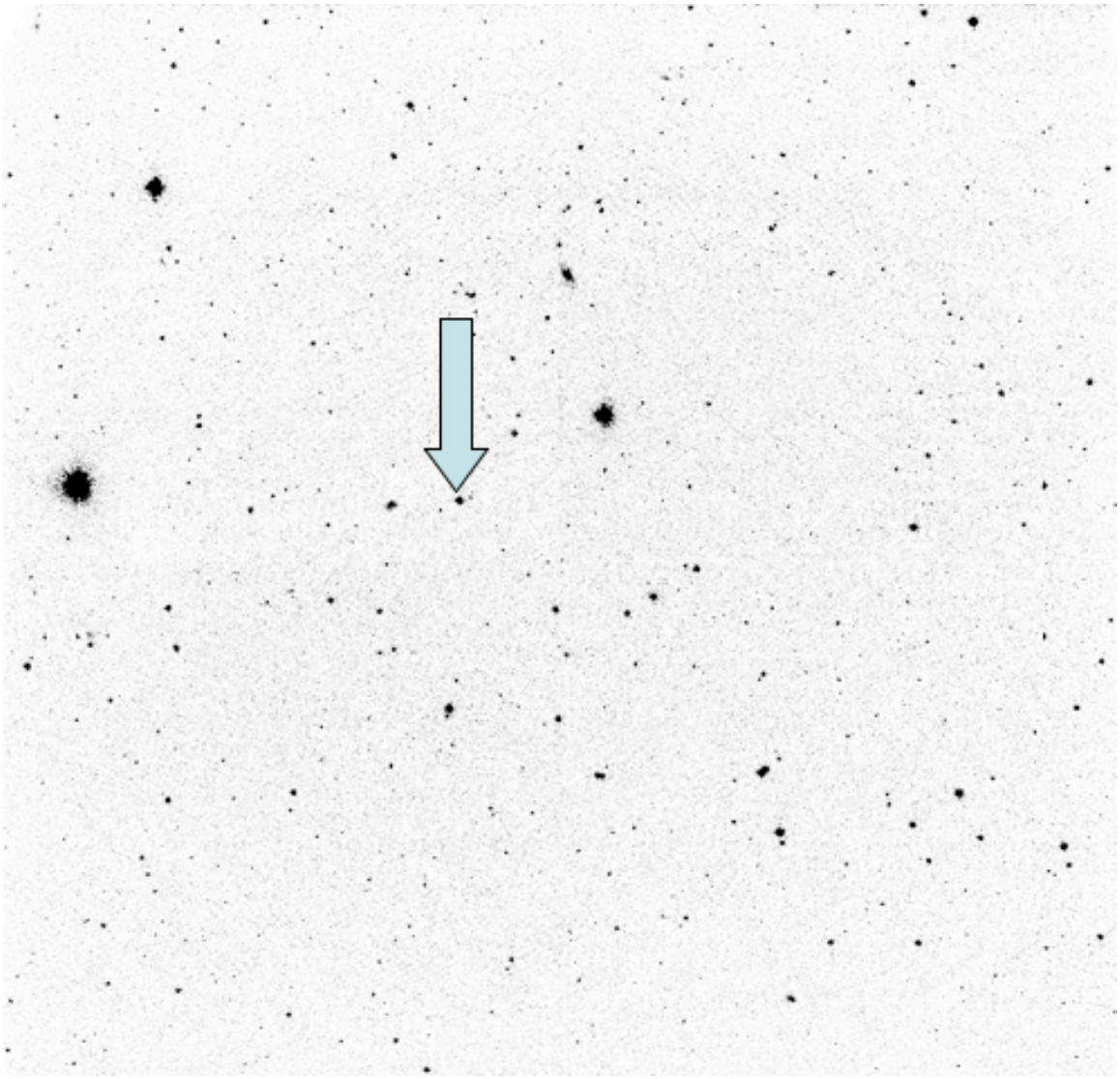

Figure 5 – Example reduced image from 23 November 2006. PKS 0537-441 is below the arrow.

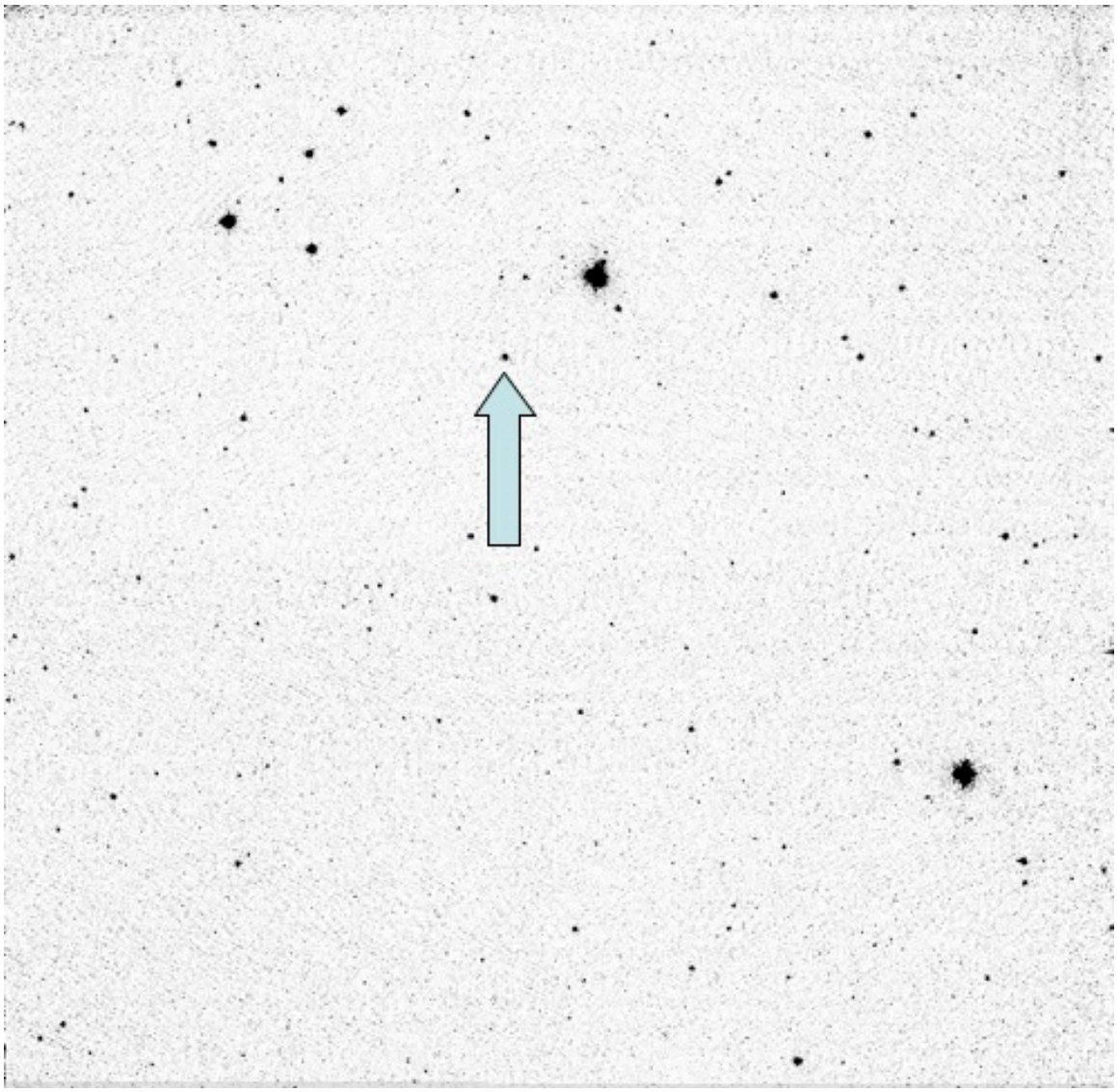

Figure 6 – Example reduced image from 24 November 2006. PKS 0447-439 is above the arrow.

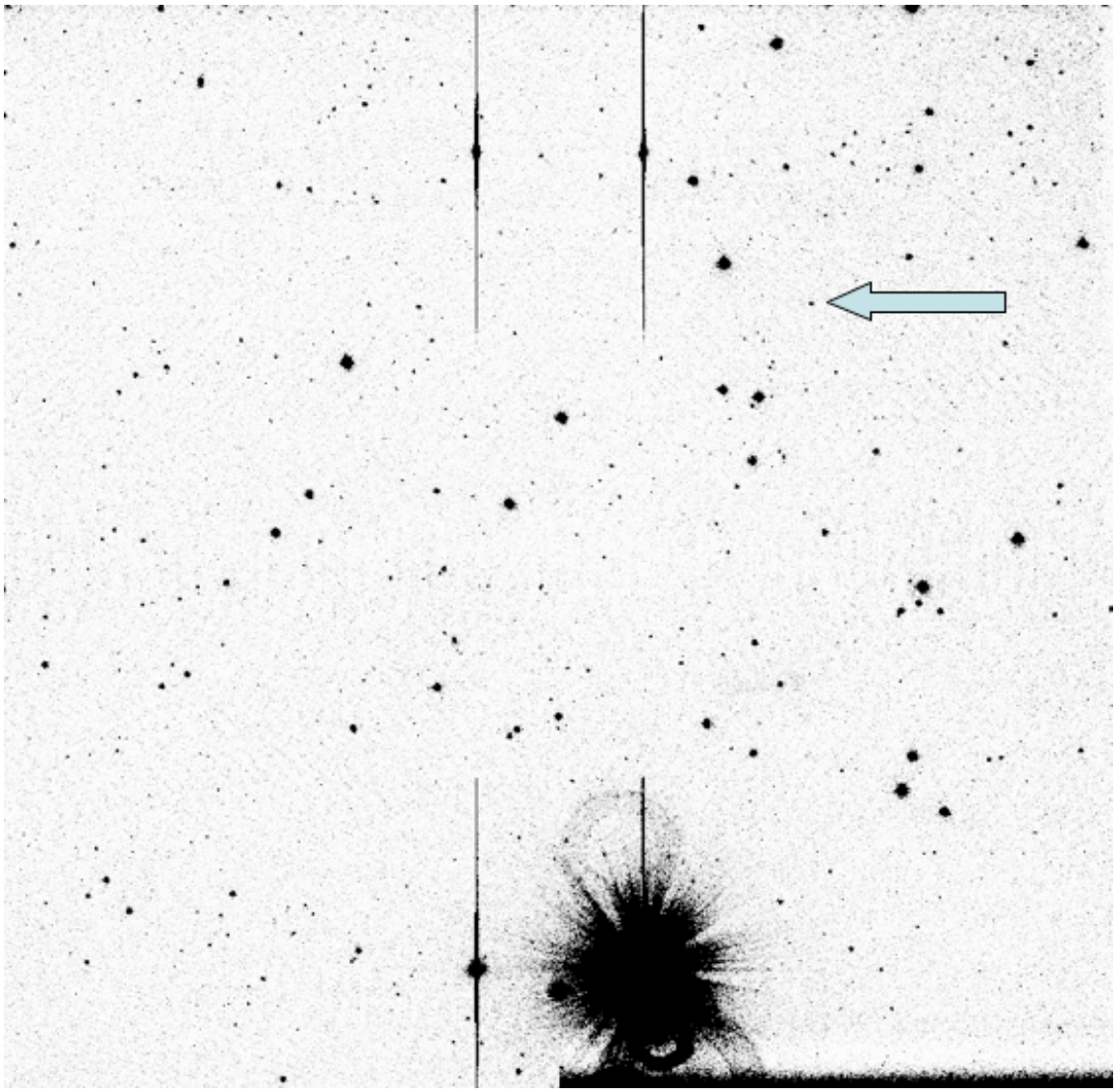

Figure 7 – Example reduced image from 25 November 2006. PKS 0208-512 is left of the arrow. The large object at the bottom is a highly overexposed star. Luckily, PKS 0208-512 is placed in the image such that the overexposed star posed no problem.

Analysis and Results

Comparison Stars

Analyzing data requires comparing our blazar to comparison stars. The point being, if we look at the blazar in isolation, it is impossible to know if any variations we see are intrinsic to the blazar, or are some type of systematic problems with the detector system or data reduction. As such, we compare the blazar to various comparison stars spread out throughout the field of view.

In principle, we want all stars to have constant observed brightness throughout the night. If a star is non-variable, its intrinsic light curve will be flat. Any deviations we see are systematic to the observing conditions. Every comparison star should show the same systematics, which means their comparison ratio should be flat. If not, there are data problems.

In creating our light curves, we use many comparison stars, such that if any show variable comparison ratios we may discard them. That does not mean the stars we keep are perfectly flat, or show no variation. We do, in fact, see a degree of variation in every star. But, if all the stars vary in the same manner, we can assume the cause is some systemic data reduction artifact, rather than intrinsic variation. In this case, we can still successfully compare the blazar to the comparison stars, because we assume the blazar also has the same systemic data reduction artifacts. The blazar must show variations greater than the residual artifacts to be considered real.

Table 3 is a list of comparison stars, and why we removed them from our analysis.

Target Object	**Omitted Star**	**Reason Omitted**
PKS 0537-441	Star 5	Dimming
	Star 6	Anomalous stray points
	Star 7	Error bars too big (very dim object)
	Star 9	Anomalous stray points
	Star 10	Anomalous stray points
	Star 11	Error bars too big (very dim object)
PKS 0447-439	Star 1	Not continuous
	Star 7	Rainbow shape
	Star 8	Too much spread
PKS 0208-512	Star 1	Missing data
	Star 2	Too much spread, anomalous stray points
	Star 3	Strong periodicity
	Star 6	Too much spread

Table 3 – Omitted comparison stars

Telescope Malfunctions

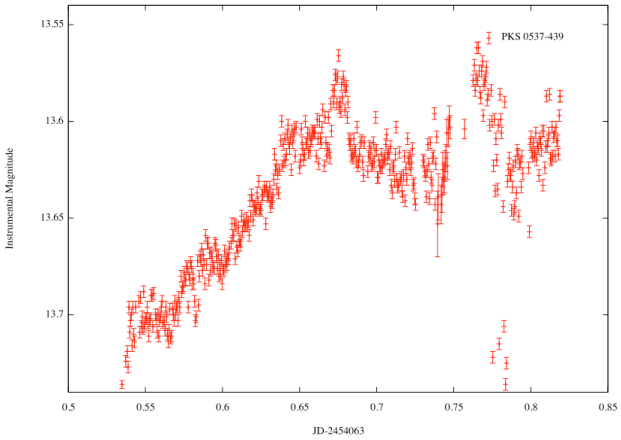

Figure 8 – Full night of data from 23-11-2006

We experienced telescope malfunctions while observing PKS 0537-441 on 23 November 2006. Figure 8 shows the full night's light curve. As can be seen, the data becomes erratic halfway thorough the observation run. According to the observation log, there was a power glitch and the dome stopped tracking. We rebooted computer systems and manually moved the dome before continuing. As the dome stopped tracking, it partially blocked light from the telescope. Though we first believed the data was salvageable, we had difficulty reconciling data after 0.669 JD, which is when the glitch occurred. At the time, we believed we fixed the problem, however, our data still show large error bars and we simply do not trust anything after the initial power glitch. Therefore, the analysis of PKS 0537-441 does not include anything data after the power glitch at 0.669 JD.

Light Curves

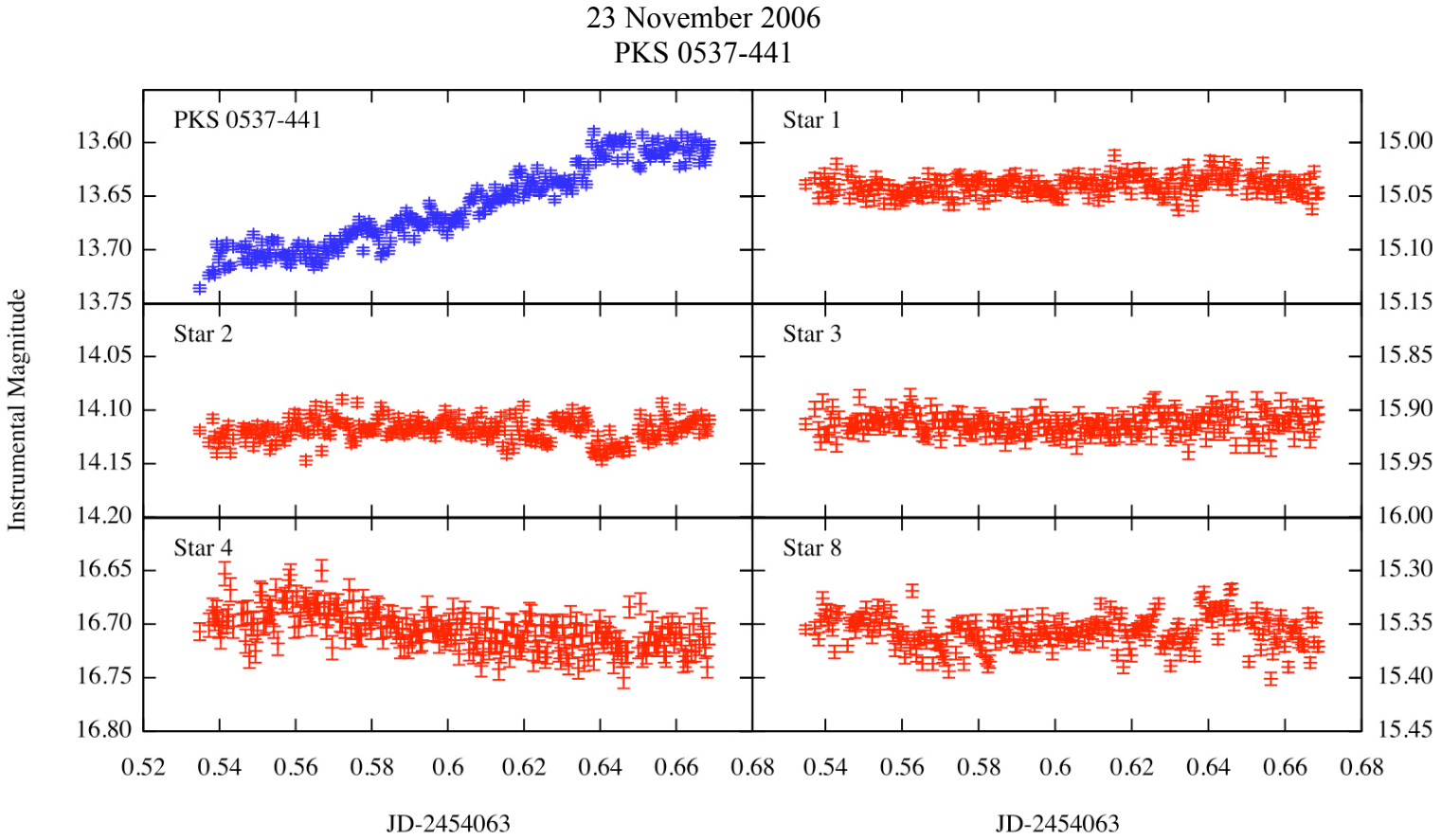

Figure 9 – Comparison of PKS 0537-441 and flat stars at 1 FWHM. Note: all vertical scales are the same size.

The above light curves compare our target blazar, PKS 0537-441, with five comparison stars. As we have not calibrated to an absolute scale, all magnitudes are relative.

We see the blazar's magnitude decrease (brightness increase) relative to the comparison stars. Star 4 shows the largest spread in this time period of about 0.1 magnitudes. We can trust blazar variations larger than star 4's spread. The blazar changes almost 0.2 magnitudes, indicating real changes in this time period. PKS 0537-439 shows clear microvariability.

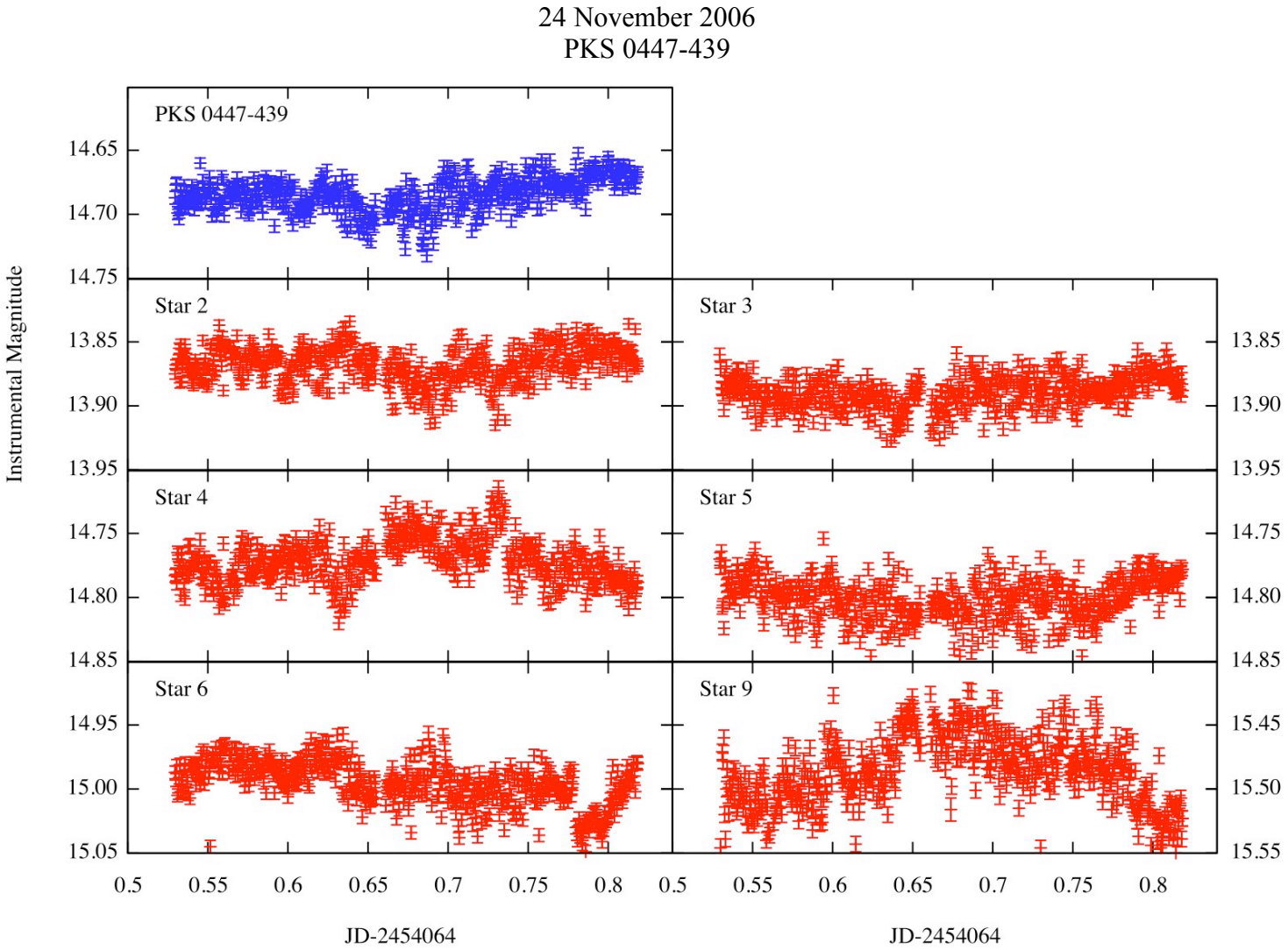

Figure 10 – Comparison of PKS 0447-439 and flat stars at 1 FWHM. Note: all vertical scales are the same size.

The above light curves compare our target blazar, PKS 0447-439, with seven comparison stars. As we have not calibrated to an absolute scale, all magnitudes are relative.

All eight objects show similar magnitude variations over the span of observations. Comparison stars 2, 3, 5, and 6 dim about 0.05 magnitudes halfway through observations. Stars 4 and 9 brighten about 0.05 magnitudes at the same time. As such, we cannot trust variations below 0.5 magnitudes as real changes. I would also be skeptical of variations occurring at precisely the same time as the variations seen in the comparison stars.

PKS 0447-439 dims about 0.05 magnitudes at the same time the comparison stars show changes. As such, we cannot trust the dip in PKS 0447-439's light curve as real. It shows no microvariability.

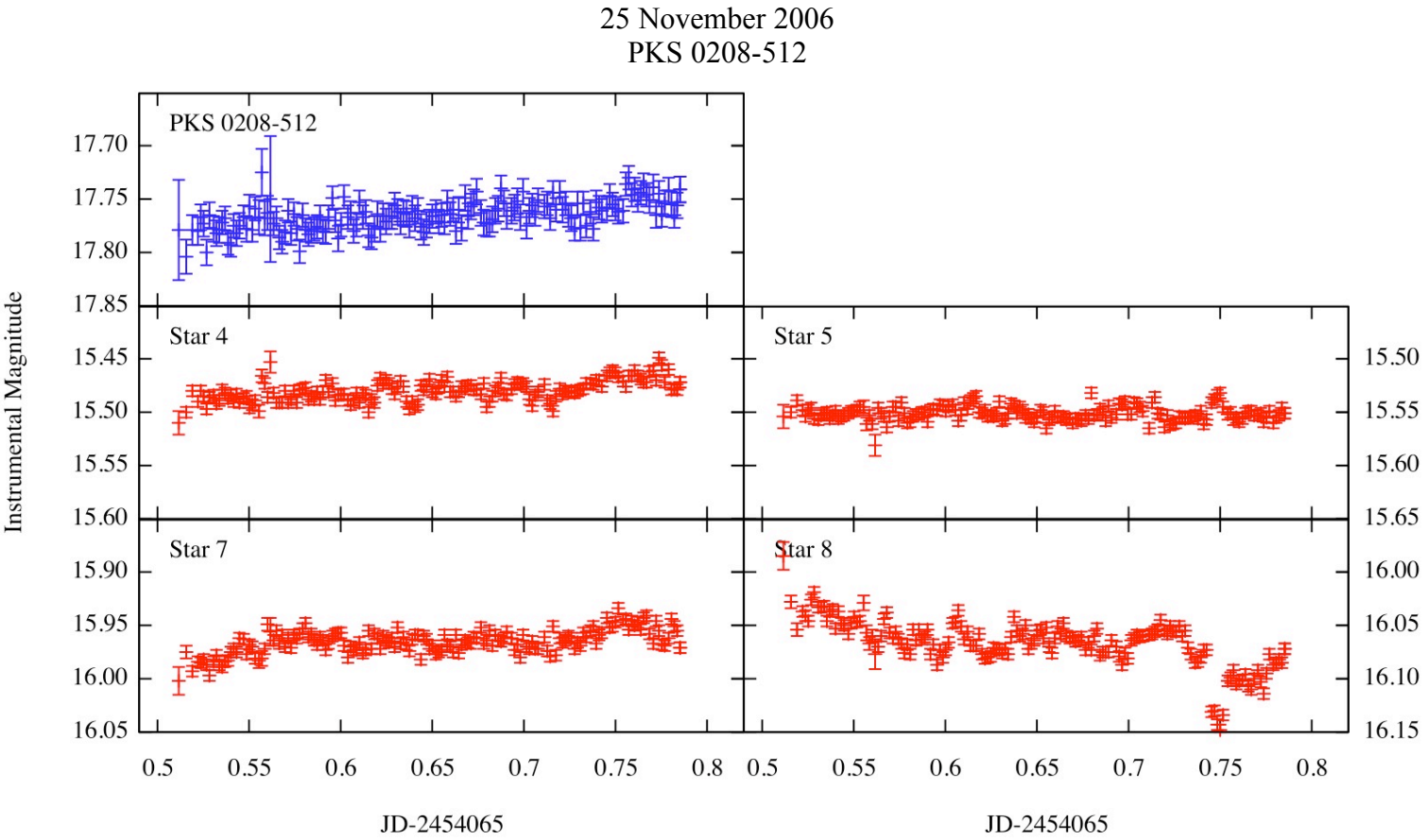

Figure 11 – Comparison of PKS 0208-512 and flat stars at 1 FWHM. Note: all vertical scales are the same size.

The above light curves compare our target blazar, PKS 0208-512, with six comparison stars. All seven objects are on the same relative magnitude scale over the same period of time.

Stars 4 and 7 show slight rises in brightness over the course of the night. Star 8 dimmed slightly and showed stray data at the end. The largest variation is about 0.05 magnitudes, and as such we cannot trust variations in the blazar smaller than 0.05 magnitudes. Star 5 shows a very flat light curve with nice error bars. Compared to star 5 alone, PKS 0208-512 appears to show a gentle rise. However, PKS 0208-512 does not show the same rise against any other comparison star, so we are very hesitant to believe it showed microvariability.

PKS 0208-512 shows the same 0.05 magnitude variations as stars 4, 7, and 8 over the course of observations, while only appearing to vary against star 5. Therefore, PKS 0208-512 most likely shows no microvariability.

Power Spectrum Analysis

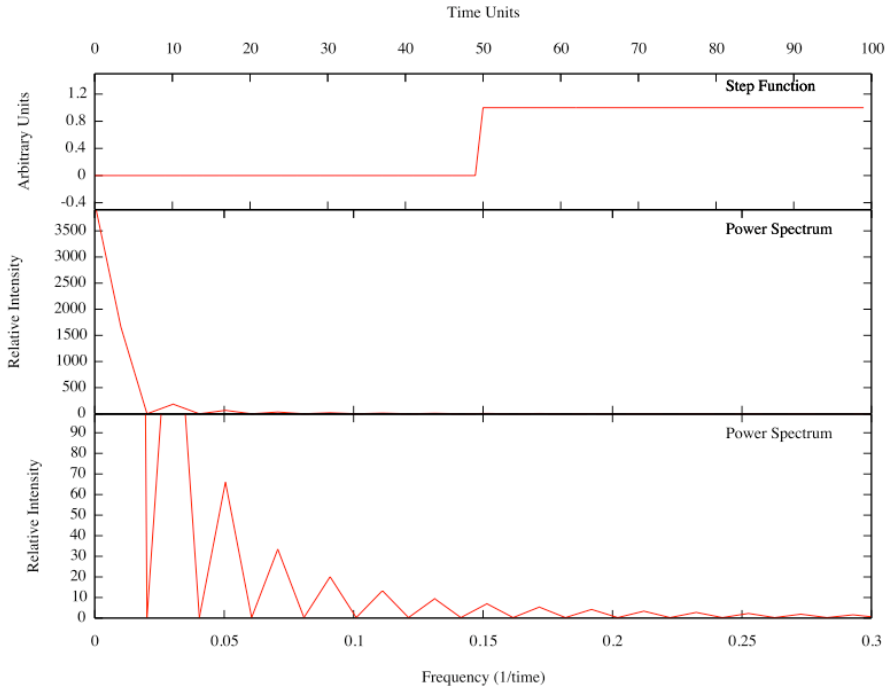

Figure 12 – Step functions and ringing. The step function is the top graph, the middle graph shows the full power spectrum, and the bottom graph gives the same power spectrum in more detail at a smaller scale. Notice the "ringing" features in the bottom figure.

While examining light curves by eye may provide insight into intensity variations, Dr. Knop and I decided to attack the data quantitatively. We performed Fourier Transforms on our data to create power spectra. To do so, we wrote a C++ code using the Fast Fourier Transform feature of the GNU Scientific Library.

Fourier Transforms recreate data with long series of sine or cosine functions. Power spectra are complicated beasts. In order to understand them better, I performed some tests using pre-made, well-defined fake light curves. I began with a simple step function, shown at the top of figure 12.

In the power spectrum, we see a large drop off with some type of decaying function as frequency increases. Inspection of the decay shows a series of declining peaks seen in the middle and bottom of figure 12. We call this "ringing," which is a windowing feature and is the expected output of a Fourier transform performed on a boxcar (step up then step down) function. If the flare or jump extended backwards and forwards forever, the power spectrum would not be windowed, would show a sharp peak, and we would not expect to see ringing.

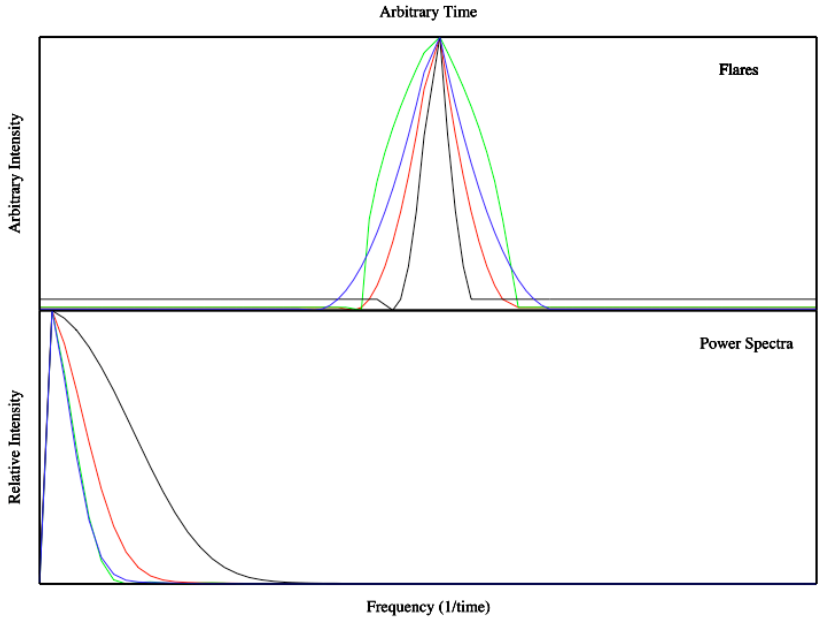

Figure 13 – Many flares and their resultant power spectrum. Colored flares correspond to the same colored power spectra. Note the shortest (thinnest) flare, the black line, has the broadest power spectrum, while the fattest flare, the green line, has the smallest power spectrum. Shorter timescale variations show more power at high frequencies.

Moving on to something that more closely resembles real data, the flares in figure 13 vary more than the previous step function. We once again see the initial large drop off in the power spectra. It is important to note that while power spectra from flares appear similar to what we saw in figure 12, flares produce power spectra that do not decay and ring, but rather spike and show smooth drop offs. Note that as the flares get larger, the power spectra show faster drop offs with more power concentrated at lower frequencies. Long flares require more low frequencies than high frequencies to construct through Fourier transforms. Conversely, short flares require more high frequencies than low frequencies to construct through Fourier transforms.

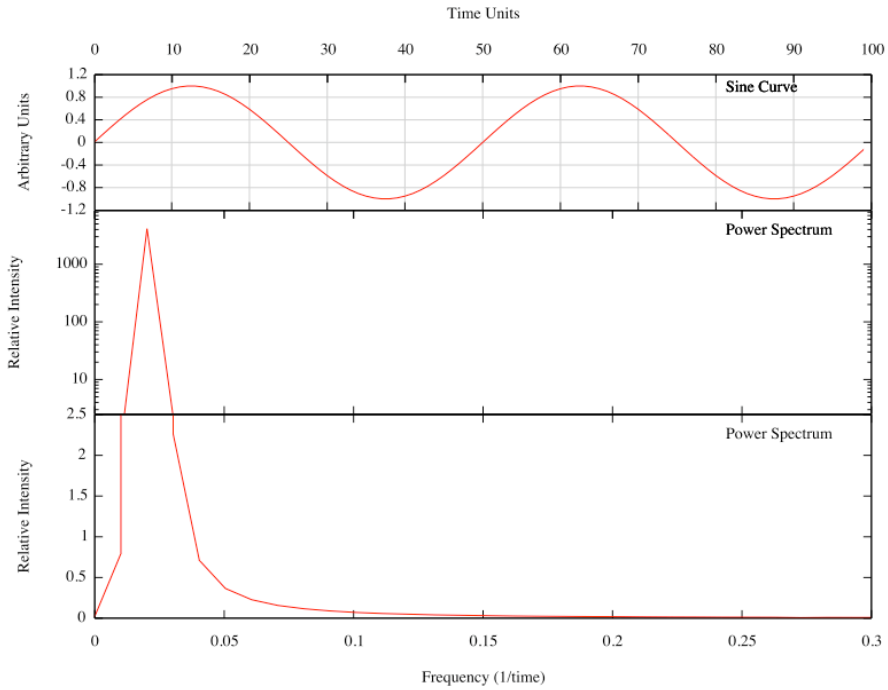

Figure 14 – Sine curve with power spectrum. The top graph shows the sine curve, while the middle graph shows the top of its power spectrum in logarithmic scale. The bottom graph shows the bottom of the peak in normal scale.

We now look at periodic data. Figure 14 shows a sine curve and its power spectrum. The curve has a period of 50 arbitrary units. Breaking it down into a power spectrum reveals a peak at 0.02 inverse periods, after which the graph levels out. As we expected, the power spectrum peak has similar shape to those in figure 13, but is much sharper because the data was made of only one frequency, rather than the many required for flares. We find that the inverse of the peak intensity, is $(0.02)^{-1} = 50$, which is the period of the original sine wave. Therefore, the position of any peaks we find in our power spectra refer to the inverse period of actual variations in our light curves.

From these examples, we may garnish three important features of power spectra. 1) The initial large drop off is a windowing feature and is to be expected in the blazar data. 2) Faster variations (sharp flares) output more power in higher frequencies. 3) The horizontal axis represents the inverse period (i.e. frequency) of variations in the data.

Blazar Power Spectra

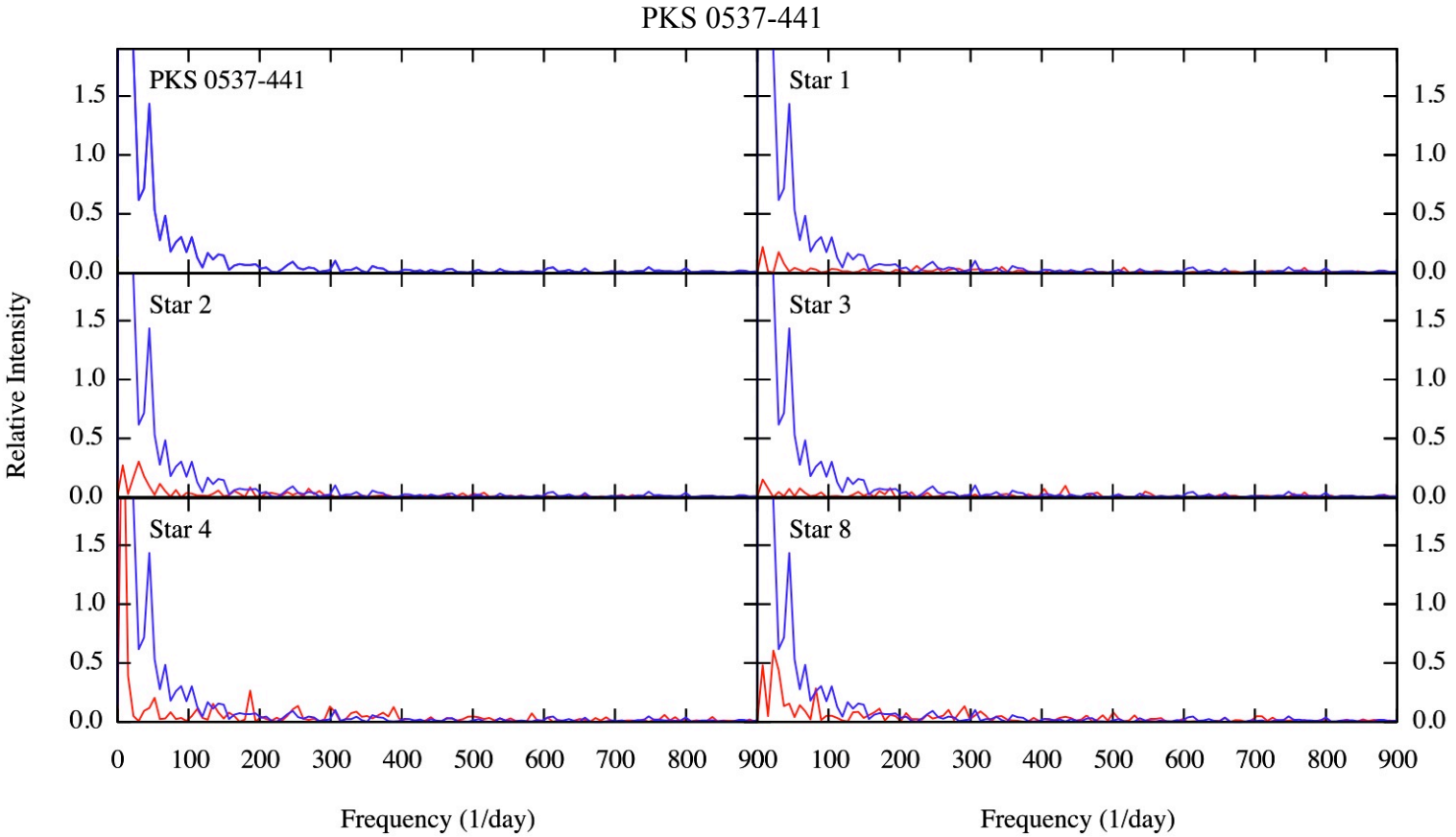

Figure 15 – Power spectra of PKS 0537-441 and comparison stars. We transposed the blazar's power spectrum in blue over each comparison star to make comparison easier.

Shown in figure 15 are the power spectra of blazar PKS 0537-441 and its comparison stars. It becomes immediately obvious that PKS 0537-441 frequently showed more variation than any of its comparison stars. As discussed above, the first large drop comes from normalizing the power spectrum to a certain base level. After the first large drop, we see a series of smaller oscillations. Both the blazar and comparison stars show oscillations on about the same level, below which we cannot trust any intensity spikes as being real variability.

PKS 0537-441 shows a prominent spike at 45 day^{-1}, corresponding to a period of 0.02 JD, or 32 minutes. No comparison star shows the same feature. Figure 16 outlines the possible variability source.

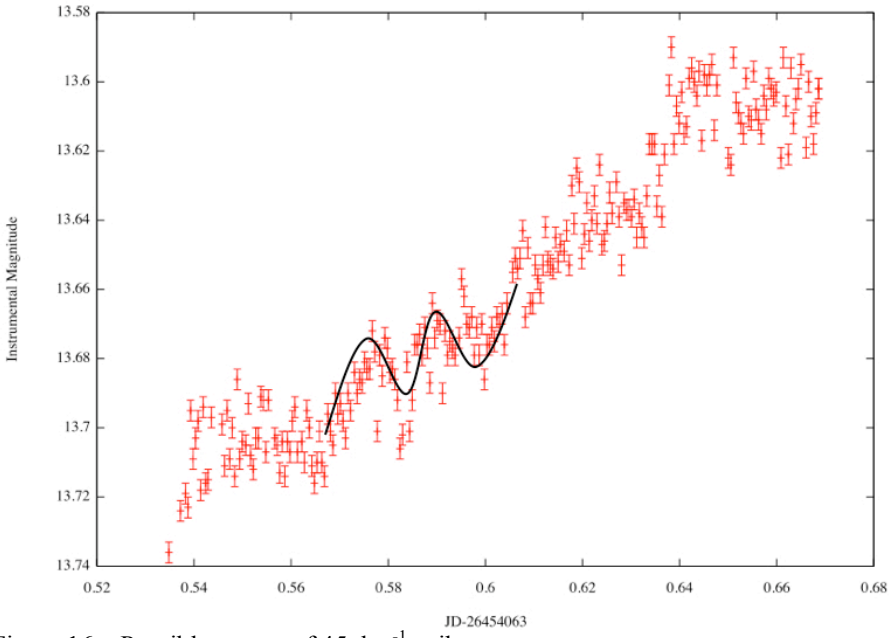

Figure 16 – Possible source of 45 day^{-1} spike.

The light curve might show wiggles inside the overall rise. However, it is entirely possible the spike is a windowing effect. Further analysis is necessary for confirmation. The power spectrum of PKS 0537-441 still remains comfortably above its comparison stars until a frequency of 100 day^{-1}, or a period of 0.01 day (14 minutes). We would need to do more analysis to verify that it is not another artifact of windowing and represents real variations. Regardless, PKS 0537-441 clearly shows microvariability.

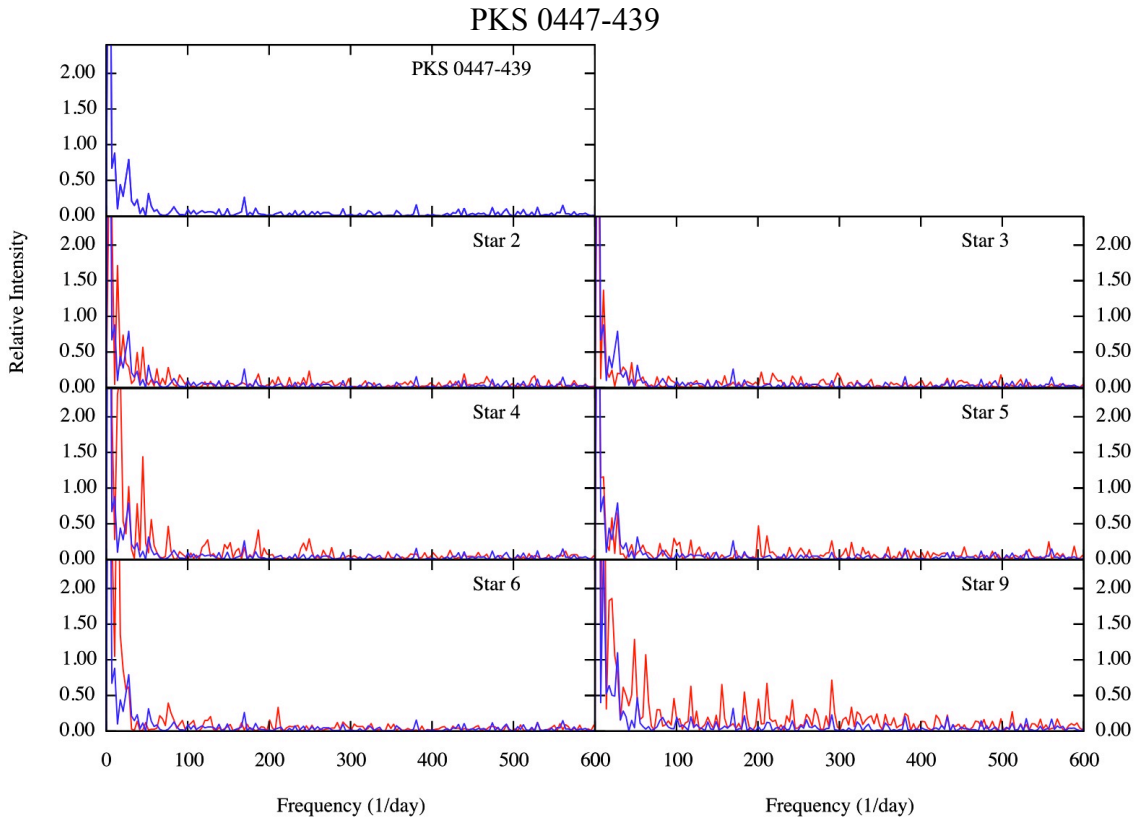

Figure 17 – Power spectra of PKS 0447-439 and comparison stars. We transposed the blazar's power spectrum in blue over each comparison star to make comparison easier.

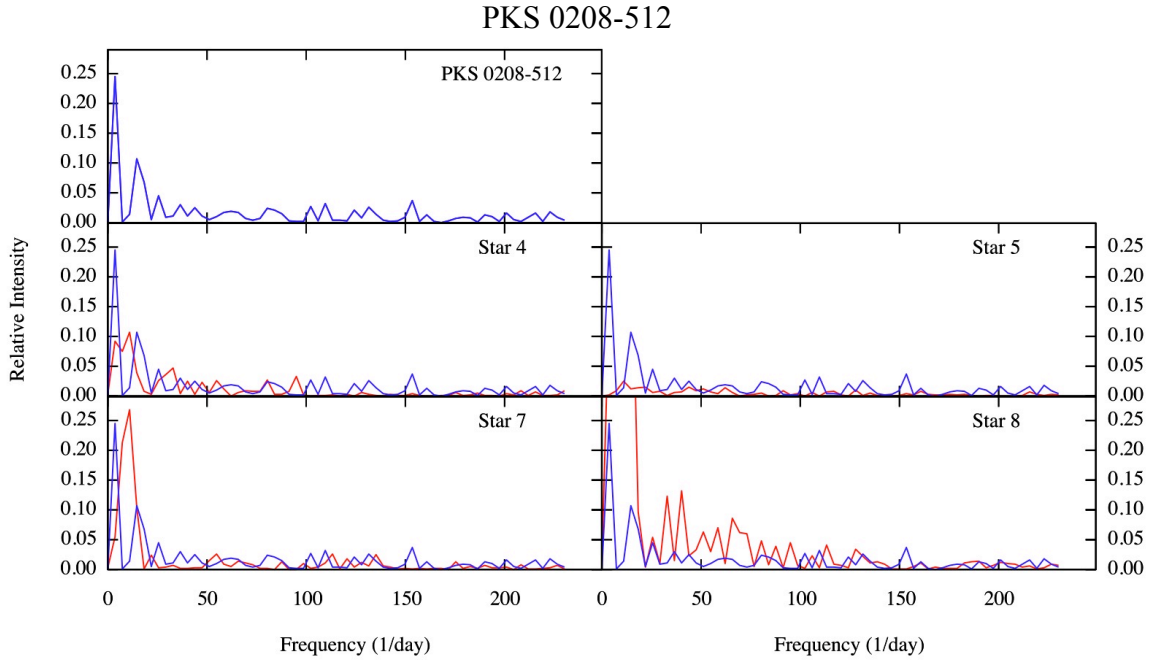

Figure 18 – Power spectra of PKS 0208-512 and comparison stars. We transposed the blazar's power spectrum in blue over each comparison star to make comparison easier.

Shown in figures 17 and 18 are the power spectra of blazars PKS 0447-439 and PKS 0208-512 as well as their respective comparison stars. By comparing relative intensities, we find that PKS 0447-439 shows a comparable level of variation to its comparison stars, if not less variation, which indicates no microvariations. For the most part, PKS 0208-512 also seems to show comparable levels of variation. However, when compared to star 5 (in figure 18), we find PKS 0208-512 shows more low frequency intensity, which we would expect after seeing it rise slightly against the light curve of star 5 in figure 11.

Power spectra comparison reiterates what we saw in the light curves of PKS 0447-439 and PKS 0208-512. We do not see microvariations in PKS 0447-439 and most likely do not see them in PKS 0208-512 either.

Conclusion

Out of the three objects we surveyed, only PKS 0537-441 overwhelmingly showed microvariability. PKS 0208-512 showed microvariability against only one comparison star, and as such we strongly hesitate to believe it actually did vary.

We explored the features of power spectra by analyzing well-defined fake data. We learned that intensity spikes correspond to periodic variations with periods that are the inverse of the locations of said spikes. However, Fourier transforms are complex. Often, artifacts creep into power spectra.

We confirmed microvariability of PKS 0537-441 through power spectra, which showed that the blazar indeed showed more variation than flat comparison stars. The power spectra also revealed higher period variability we may not have noticed by examining light curves alone. If the prominent peak at 45 day^{-1} is to be believed, then we may narrow the variable region of the AGN to a size less than 32 light minutes or 4 AU. We also notice that the power spectrum of PKS 0537-441 shows more power than its comparison stars out to 100 day^{-1}, which corresponds to a size of 14 light minutes or 1.75 AU. Further analysis would be required, however, to verify the higher regions of the power spectrum are not windowing features, but physical variability.

Future Work

The next step for this research would be to examine PKS 0537-441 over longer time scales. As we most likely did not observe a complete variable period, longer observations would give a much better idea of the nature of PKS 0537-441's variability. Conversely, we would also like to see more detailed, faster observations of PKS 0537-441 to determine the validity of periodicity on fast time scales inside the overall rise. Also, more observations of PKS 0208-512 would reveal whether or not the variations seen against one comparison star were a fluke or represent a real phenomenon.

References and Acknowledgements

Acknowledgements

Dr. Robert Knop
Dr. David Weintraub
Dr. Andreas Berlind
Dr. Charles Macguire
Vanderbilt University Department of Physics and Astronomy
My fellow classmates
My family
My friends

References

Dolcini, A., et al., A&A, 443, 33

Ghosh, K. K., Ramsey, B. D., Sadun, A. C., Soundarajaperumal, S., Wang, J., 2000. ApJS 127, 11

Jensen, A., 2008, Vanderbilt Undergraduate Honors Thesis

Krauss, A., Witzel, A., Krichbaum, T. P. 1999, New Astron. Rev., 43, 685

Krolik, Julian H. *Active Galactic Nuclei*. Princeton, New Jersey: Princeton University Press, 1999.

Meier D. L., Koide S., Uchida Yu., 2001, Sci, 291, 84

Pogge, R., SMARTS Consortium CTIO Yale 1-meter Telescope & Y4KCam. [http://www.astronomy.ohio-state.edu/Y4KCam/detector.html] Updated: 12/2007

Romero, G. E., Cellone, S. A., Combi, J. A., Andruchow, I., 2002, A&A, 390, 431

Romero, G. E., Cellone, S. A., Combi, J. A., 2000, AJ, 120, 1192

Simonnet, A., Sonoma State University. [http://universe.sonoma.edu/~aurore/]

Wagner, S. J., Witzel, A., 1995. ARA&A, 33, 163

Wiita, P. J. 1996, in Blazar continuum Variability, ed. H. R. Miller, J. R. Webb, J. C. Noble (San Francisco: ASP), ASP Conf. Ser., 110, 42